environmental microbiology

Environmental Microbiology (2014) **16**(1), 118–129 doi:10.1111/1462-2920.12216

Foraging by a wood-decomposing fungus is ecologically adaptive

P. R. Darrah* and M. D. Fricker
Department of Plant Sciences, University of Oxford, South Parks Road, Oxford OX1 3RB, UK.

Summary

We show that fungi that forage for wood do not conform to the paradigm of symmetric radial growth and grow asymmetrically by default. Asymmetry is further accentuated by contact with a resource that also partially polarizes growth in the direction of the resource. Despite marked changes at the perimeter, overall growth allocation on an area basis is, however, unchanged implying sophisticated regulation at the colony level. Using mathematical models, we show that this behaviour is best explained as a local response of the immediate segment contacting the resource. The model reveals that foraging behaviour is adaptive but only for resources that are clustered in space and is selectively neutral for randomly scattered resources. This clustered spatial distribution matches that found in the natural environment. Modelling also shows that the foraging strategy used by these fungi involves substantial risks as well as benefits.

Introduction

Most organisms live in environments where the resources they require are heterogeneously distributed in space and/or time (Hutchings *et al*., 2000). To survive, they must search for them and evolutionary forces are expected to optimize any resulting foraging strategy (Pyke, 1984). Deriving from the seminal paper of MacArthur and Pianka (1966), foraging strategy is now a very well-developed field of ecology. As a general rule, animals concentrate on the exploration of space (James *et al*., 2011) while plants concentrate on the occupancy of space (Lynch and Brown, 2012). Space occupancy is typically plastic in response to localized conditions with, for example, selective root placement in response to heterogeneous conditions (de Kroon *et al*., 2005). The fungal case may be intermediate. Like plants, filamentous fungi forage by laying down structures to explore space and respond to heterogeneous conditions (Boddy, 1999) – but the structures may be more transient leading to a more 'mobile' morphology (Rayner and Franks, 1987; Fricker *et al*., 2009).

Basidiomycete fungi are among the most important recyclers of photosynthetic carbon in forest ecosystems (Watkinson *et al*., 2006). Those that feed on discrete woody material experience patchily distributed resources and therefore must search their environment to find them (Fricker *et al*., 2008). Fungal foraging in woodland can take two forms – the fungus can occupy space to capture new resources falling from above and/or it can explore new areas to search for resources already on the forest floor (Boddy *et al*., 2009): we investigate the latter exploratory form in this paper. This exploratory growth can involve short-range foraging typified by species such as *Hypholoma fasciculare* and *Stropharia* spp. or longer-range foraging as typified by *Phanerochaete velutina* and *Resinicium bicolor* (Boddy *et al*., 2009). Short-range foragers typically exhibit diffuse and slowly growing colony margins and forage for relatively homogeneous resources. Longer-range foragers are often corded and fast growing, with a relatively lower fractal dimension and forage for more sparsely distributed resources. In both cases, plastic responses could increase foraging success, but the potential is greater for the longer-range foragers because of their sparse resource distribution, and we concentrate on this group in this paper. The behaviour of these fungi once a resource is contacted can be quite complex (Dowson *et al*., 1986; 1988), but here we concentrate just on the response at the colony margin.

Filamentous fungi grow by tip extension and branching, which tends to form radial colonies (Prosser and Trinci, 1979) with an indeterminate spatial scale (Agerer, 2001). For explorative foraging to be adaptive, this radial symmetry must be broken via changes in growth rate (GR) over portions of the periphery – over time these translate into changes in colony shape by generating convex bulges or convexities. If these convexities form in response to environmental stimuli and they are adaptive, i.e. by adopting them the fungus acquires more resources

Received 2 April, 2013; revised 9 July, 2013; accepted 14 July, 2013.
*For correspondence. E-mail peter.darrah@plants.ox.ac.uk; Tel. (+44) 1865 275124; Fax (+44) 1865 275074.

and an increased fitness, then the fungus can be said to have a foraging strategy.

Our hypothesis is that wood-consuming basidiomycete fungi, as represented by *P. velutina*, do not simply passively explore their surroundings, but actively forage by sensing the presence of woody resources in the environment and responding adaptively to them. We assume that the fungus cannot sense the resource from a distance and that contact is required for the fungus to register its presence. To test this hypothesis it is necessary to demonstrate that:

i. Fungi can respond in a directional manner to the presence of a suitable resource.
ii. That the directional response is adaptive, i.e. it would lead to superior fitness in the organism deploying it. We used resource capture as a surrogate for fitness in this study.

These two hypotheses were investigated by observing the perimeter responses of a fungus, which was challenged with randomly positioned resources, of nutritional and non-nutritional benefit. We predicted that only nutritional resources would elicit a directional response. We then used simulation models to investigate to what extent a directional response would be adaptive and lead to superior fitness.

Results

Colonies broke radial symmetry in all conditions

To test whether nutrient-stressed *P. velutina* obeyed the paradigm and grew symmetrically, we grew the fungus across a nutrient-deficient surface – it did not. Figure 1A shows typical convexities in a composite image – two perimeter bulges were observed with a generally asymmetric looking colony.

Before resources were added to the cultures, 36 convexities were detected generated by 25 of the 42 colonies investigated. After cellulose resources (FP) were added to 15 colonies, 38 additional convexities were identified while 39 additional convexities were identified in the 13 samples treated with inert (glass fibre) resources (GF). Therefore, both treatments generated about three convexities per colony. In unbaited samples of the same age as baited ones, only six additional bulges in total were found for the eight colonies examined, and these were not included in the statistical analyses. These observations suggest that the additional convexities observed after resource addition were in direct response to the addition rather than being a function of colony age. More convexities were detected during time series analysis than the composite analysis because some were both small and transient – 54 and 47 were detected after resource addition for FP and GF baits respectively.

The conventional fungal paradigm is symmetric radial growth (Trinci, 1971; Prosser and Trinci, 1979). When grown across a more ecologically realistic inert surface, we found that colonies were almost always asymmetrical with pronounced multiple bulges. This asymmetry did not depend on the presence of a resource. Perimeter convexities must require enhanced perimeter growth rates, and we assume that this is a local response involving part of the perimeter becoming excited into faster growth. Differential resource allocation to the local region to drive the growth is also possible but would require a more complex model to explain. The asymmetry has the effect of increasing the colony perimeter for the same area and may represent an adaptation for contacting more resources at comparable cost.

The resource stimulus induced more asymmetry and a wider dominant convexity

To understand the differences in the nature of the response to the addition of different resource types, we characterized the convexities in terms of their angular

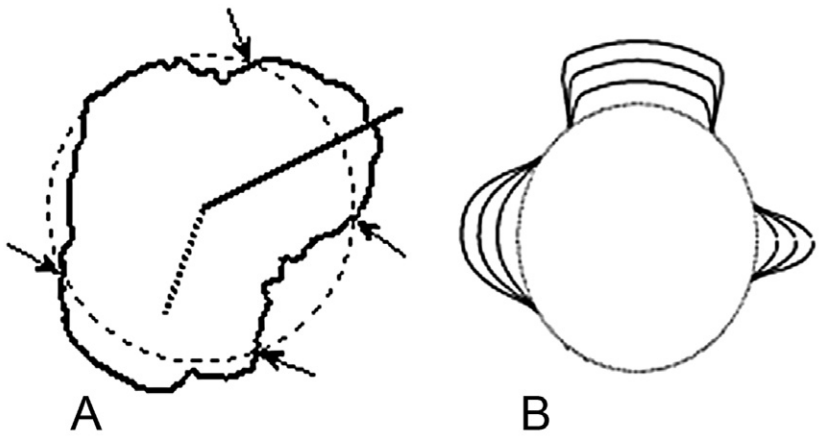

Fig. 1. A. Representative composite image of the perimeter of a fungal colony provided with a cellulose resource: the solid line represents the average colony perimeter since resource addition while the dotted circle shows a symmetric colony with the same area. Arrows indicate the position of bulges identified by the peak detection algorithm. The dotted line arising from the origin shows the direction of the centre of the dominant bulge, and the solid line indicates the direction of the added resource.
B. Simulated bulges generated by the three-parameter mathematical models (see text) showing how flexible the perimeter can be with a simple model. For each convexity, the three different lines denote three different times since the bulge was initiated.

Table 1. Characterization of dominant (d) and subdominant (s) convexities in composite perimeters from colonies baited with cellulosic (FP) or glass fibre (GF) paper.

	Relative length	Angular width (°)	Growth rate (mm h^{-1})	Relative growth rate
Mean FP-d	1.31 ± 0.04	97.8 ± 9.2	0.241 ± 0.035	3.01 ± 0.95
Mean FP-s	1.17 ± 0.02	40.5 ± 6.2	0.144 ± 0.030	1.59 ± 0.41
Mean GF-d	1.28 ± 0.03	62.0 ± 5.0	0.247 ± 0.038	2.08 ± 0.65
Mean GF-s	1.2 ± 0.03	39.8 ± 6.0	0.153 ± 0.029	1.25 ± 0.22
d vs. s FP + GF combined	t = 5.06, df = 75	t = 8.01, df = 75	t = 4.97, df = 99	t = –4.26, df = 99
	$P < 0.0001$	$P < 0.0001$	$P < 0.0001$	$P < 0.0001$
d-FP vs. d-GF	t = 0.75, df = 26	t = 4.42, df = 26	t = 0.28, df = 26	t = 1.34, df = 26
	$P = 0.458$	$P = 0.0002$,	$P = 0.781$	$P = 0.191$
s-FP vs. s-GF	t = –1.93, df = 47	t = 0.136, df = 47	t = 0.35, df = 71	t = 1.08, df = 71
	$P = 0.059$	$P = 0.98$	$P = 0.731$	$P = 0.22$

Means are shown with 95% confidence intervals. Parameters are defined in the text.
df, degrees of freedom.

length and width. Convexities were classified as dominant (with the largest area) or subdominant for each colony (Fig. 1). The mean maximum relative lengths, LB, of convexities for dominant (1.30) vs. subdominants (1.19) were significantly different, but there were no differences between dominant or subdominant LB because of resource type (Table 1). Dominant convexities for FP had a significantly larger angular width (97.8°) than GF (62.0°) while subdominant widths were indistinguishable by resource type (Table 1).

Figure 2 shows an example of the single and biphasic regression analysis used to estimate these rates – the data were fitted very well by linear regression ($P < 0.0001$ for all analyses). Growth rates of dominant (0.244 ± 0.024 mm h^{-1}) and subdominant (0.148 ± 0.021 mm h^{-1}) convexities were significantly different from each other but not between resource type (Table 1). Convexities were normalized by the median perimeter length for each time frame – on this relative basis, FP bulges grew over three times faster on average than the median for the colony (Table 1). Overall, dominant (2.58 ± 0.60) and subdominant (1.43 ± 0.24) bulges were again significantly different with resource type again uninformative (Table 1).

Dominant convexities were more frequent in baited systems, implying that stimulation by the resource caused a section of the perimeter to become more excited. This excitation typically lasted for the remainder of the experiment, although there was some evidence of attenuation of response in some colonies. The variation among convexity length, width and GR within each class was small: the dominant and subdominant bulge form is therefore likely to be a predetermined phenotype rather than some form of stochastic perimeter response to stray environmental stimuli. The difference in angular width for dominant convexity between the baits implies that the cellulose bait provides an additional stimulus, causing more of the perimeter to become excited.

A second stimulus is required for directional responses towards the resource

To test our hypothesis that fungi can respond in a directional manner to resources, we determined the difference between the angular direction of each convexity and the resource – we would expect growth to be polarized towards the resource if the hypothesis was correct. Figure 1A illustrates this, where the dotted line shows the bait direction while the solid line shows the direction of the dominant bulge. Figure 3A summarizes all these angular differences for cellulosic baits and shows that dominant bulges tend to point roughly at the bait while subdominant bulges show a more uniform distribution. In contrast, Fig. 3B shows the equivalent diagram for GF resources where no apparent directional bias of dominant bulges was apparent.

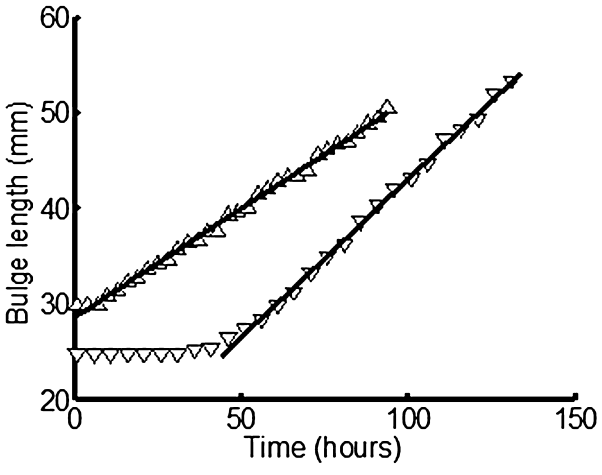

Fig. 2. Bulge length (from the colony centre) as a function of time for two different colonies following the addition of a cellulose resource. The fitted lines show the linear regression fit ($P < 0.0001$) to the growing bulge for a colony showing an immediate (monophasic) response (△) and a delayed (biphasic) response (▽) to bait addition.

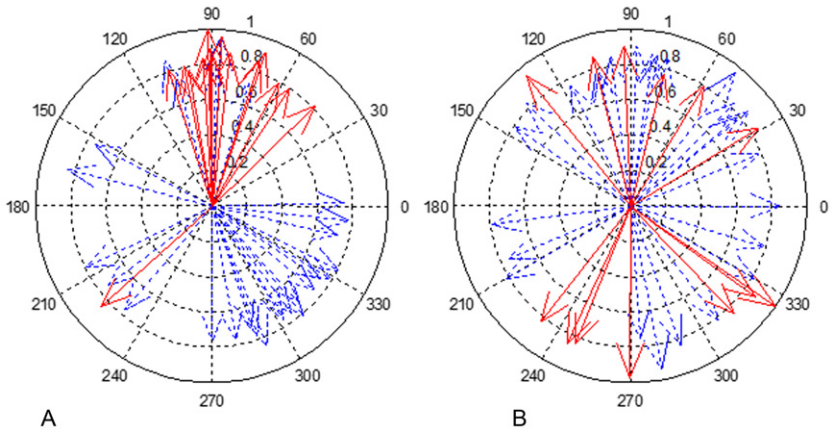

Fig. 3. The angular direction of dominant (red solid line) and subdominant (blue dotted line) bulges relative to (A) a cellulosic resource or (B) an inert (glass fibre) resource positioned at an angle of 90°.

We conducted statistical tests to determine if the observed polarizations were significantly different from those arising by chance. Table 2 shows the results of the statistical tests of the circular distributions (Mardia and Jupp, 2000). Only the dominant FP bulges showed much concentration of the angular directions, with a value of $k = 2.78$ indicative of considerable clustering around the direction of the resource. In contrast, the angular distribution of the GF-dominant bulges and the bulges detected before resource addition were close to being random samples from a uniform von Mises distribution, implying no preferred directionality. The differing clustering tests showed slightly different levels of significance, but only the FP-dominant class consistently showed a strongly significant (> 99%) result on all tests. Rayleigh's uniformity test and Rao's spacing test both strongly refuted the hypothesis that the FP-dominant bulges were distributed uniformly around the circle. The V-test is related to Rayleigh's uniformity test but tested the alternative hypothesis that the distribution is in fact non-uniform and with a mean of zero, i.e. no difference between dominant bulge direction and bait direction – the V-test also provided very strong support for the FP-dominant bulge being a directional response towards the bait.

Although FP and GF baits both induced faster growing convexities, only cellulose could orientate the dominant bulge towards the bait. This means that a second signal, possibly nutritional, was required to focus the dominant bulge onto the appropriate heading. This second signal is probably also responsible for exciting a larger section of the colony perimeter into enhanced growth.

Growth is tightly regulated at the colony, not the perimeter level

We then tested whether the fungus responded to the cellulose bait by increasing its growth rate. The mean growth rates after bait addition were 0.130, 0.131 and 0.131 mm h^{-1} for control, GF and FP treatments respectively. Analysis of variance of log-transformed GR data showed no evidence ($F_{2,28} = 0.002$, $P = 0.998$) that the rates were from different populations, indicating that growth was not enhanced by the nutrient supply.

Peripheral growth of our colonies required transport of material to the growing hyphal tips because all the nutrients available to the fungus were provided at the centre of the colony by an agar disc. Contact with a cellulosic bait, which could represent an alternative source of energy and nutrients if utilized, did not trigger an increase in colony

Table 2. Circular statistics (see text) calculated for different convexity classes from composite perimeters.

	FP dominant	FP Remainder	GF dominant	GF remainder	C	P
Number of convexities	15	29	13	26	8	25
Concentration	2.78	0.73	0	0.67	1.25	0.30
Rayleigh test	10.56***	3.38**	0.22	2.65	2.68	0.54
Rao's spacing	248.3***	154.8*	130.4	120.9	139.0	130.7
V-rest	0.84***	–0.24	–0.03	0.29	0.14	0.05

One hundred sixteen convexities were divided into four groups comprising (i) cellulose resources (FP), (ii) glass fibre resources (GF) and (iii) no resources (C) (after notional addition of baits) and (iv) all the samples before the addition of resources (P). The FP and GF convexities were further divided into dominant and subdominant bulges.
Significance at > 99% is denoted by ***, significance at > 95% by ** and significance at > 90% by *.

growth as colony GR was not significantly increased by the bait. However, the stimulus did induce a local increase in perimeter GR that was exactly compensated for by a decrease in GR elsewhere – this implies global control of colony resource allocation and sophisticated regulation of resource distribution.

Phanerochaete velutina *responds actively to the presence of woody resources with a directed perimeter response*

The experimental evidence outlined above showed that the fungus responds to contact with a nutritional resource by growing more rapidly in the direction of the resource. This enhanced growth response of part of the colony perimeter in the direction of a resource seems to indicate that *P. velutina* is actively foraging for resources. But while such a response is necessary for foraging to occur, it is not sufficient to prove that the response is a foraging strategy. To do so, it is necessary to show that more resources would be captured by adopting this response – this we do in the next sections by exploring the consequences of the response by simulation modelling.

A three-parameter growth model can generate a wide range of perimeter convexities

We built a model that could simulate a fungal colony with differential GRs around its margin, as observed in *P. velutina*. The excitable segment response (ESR) colony growth model, as detailed in Experimental Procedures, consisted of only three parameters describing (i) the maximum GR of a convexity (G) relative to uniform radial growth, (ii) the angular length of segment involved (W) and (iii) the proportion of that angular length that grew at the maximum rate (P). Despite this simplicity, the model could generate a wide range of perimeter convexities depending on the parameter values selected as shown in Fig. 1B. To constrain the model, parameters describing the size, shape and magnitude of the excitable response were taken from experimental data: these were $G = 3$, $W = 112°$ and $P = 0.47$. The spatial scale was chosen such that the dominant perimeter response on a fixed heading for the entire duration of the simulation could not exceed the unit circle. In all cases, the ESR model was compared with a model of radial symmetric growth (the uniform response or UR model): the ESR model was constrained such that the total area of the fungal colony at each time step was the same for both the ESR and UR models.

In nature, resources can be scattered in different patterns, for example, entirely randomly or randomly but with some clustering: we used the simulation model to explore the success of the fungus at acquiring resources for different resource distributions – in all cases, the success was scored relative to a non-responsive, symmetrically growing fungus. We ran many simulations using different random distributions (500 per distribution) and then aggregated the responses to predict the average success.

If the success using the foraging response was positive overall, then we concluded that the response was adaptive and the fungus would increase its fitness by deploying the strategy.

Simulated foraging behaviour is very dynamic

In the simulations, resources were scattered on the plane, and the fungus either allowed to explore the resource space using its active segment response whenever it contacted a new resource (the ESR model) or by continuing to grow radially and symmetrically (the UR model): the colony area was constrained to be the same in both models at each time step.

A typical simulation for randomly scattered resources is shown in Fig. 4. After 11 time steps, the growing colony margin contacted the first resource, and an excitable response segment was formed on a south-west (SW) heading and lying between the arrows in Fig. 5A. No new resources lay in that direction so the segment persisted for the latency period of 10 time steps and then ceased growing at the faster rate leaving the bulge shown in Fig. 4B. A second excitable response segment was then formed after 32 time steps by contact with another resource but this time in a south-east direction. This again died out and new segments were formed after 60 (north-east) and 77 (SW) time steps. This latter segment was then maintained until the end of the simulation (Fig. 4E) by repeated contacts with new resources being made within the latency period – this gave rise to the large bulge to the SW with previous bulges contributing to the overall radial asymmetry.

The pattern of resource capture is shown in Fig. 4F, which shows how the effectiveness of the two models switched over time. This instance of the model ended up capturing one more resource than the UR model, and the average capture difference was 0.19: this particular realization represented the simulation forming the third quartile point of the 500 completely spatially random (CSR) patterns investigated.

Foraging behaviour is adaptively neutral for randomly scattered resources

We tested the fitness of the fungus using the adaptive foraging strategy by counting the number of resources it acquired compared with the number acquired by the UR model when challenged with the same resource

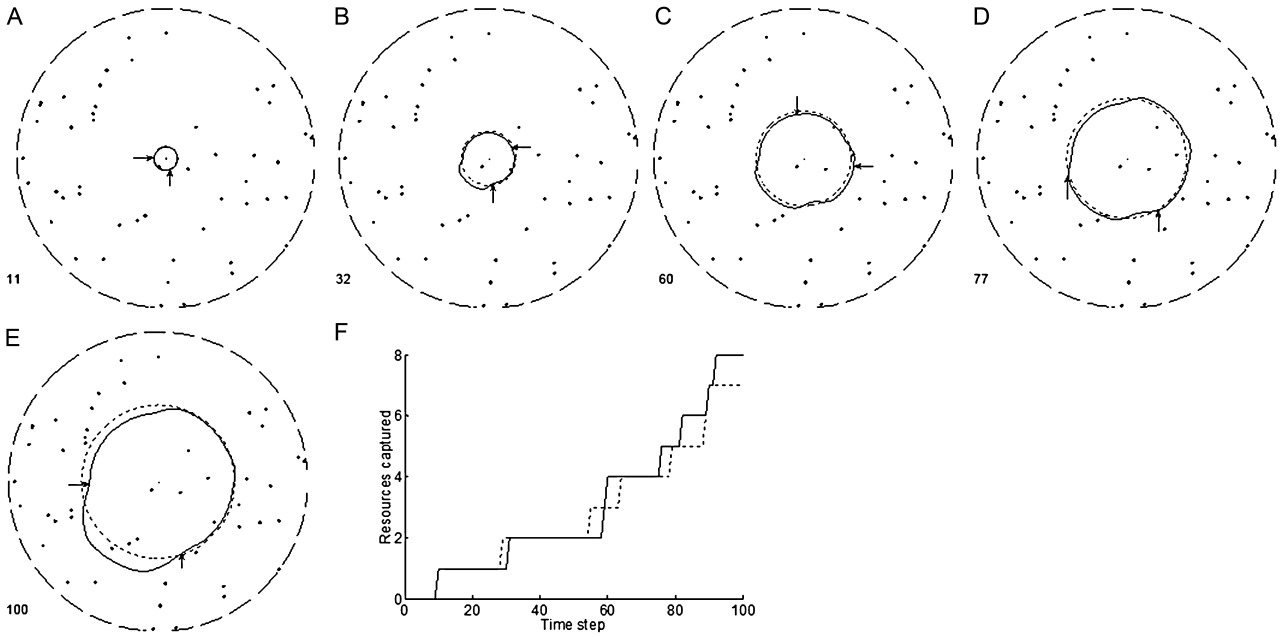

Fig. 4. Simulated development of colonies produced by the UR (dotted line) and ER (solid line) models in response to the distribution of resources produced by a single iteration of a completely spatially random algorithm. In A–E, the numbers indicate the current time step, and the arrows represent the outer limits of the excitable segment: for this simulation, the resource density was 50, the response duration was 10 and there was one bulge focus permitted per time frame. The resources captured by UR (dotted) and ER (solid) models (F) over time correspond to an average capture difference (ΔA) of 0.19 (see text).

distribution. For randomly scattered resources (CSR model), mean values for ΔA for the 27 parameter combinations ranged from −0.08 to 0.065, with an overall mean of zero (Table 3). Some spatial patterns supported more extreme outcomes with values from single runs ranging from of −4.6 to 4.6. There was no evidence that the means were significantly different from zero, indicating that UR and ESR models on average performed equally for all parameter combinations. This was confirmed when three-way analysis of variance showed that neither of the two parameters had a significant effect at any of the three resource densities (Table 3).

Completely randomly distributed resources have no predictable spatial structure, i.e. knowing the position of one resource is completely uninformative about the position of other resources. Overall, therefore, the expected outcome was predicted to be neutral with neither model performing better than the other – this expectation was realized. Some individual spatial patterns were expected to show some form of clustering by chance, and this explained the positive and negative outcomes encountered as the model was sensitive to clustering (Fig. 5A1–A3). We would predict that these patterns would show evidence of clustering if an appropriate algorithm was used (Ripley, 1976), but they could not be detected visually implying that the fungus is responding to subtle differences.

Foraging behaviour is strongly adaptive for clustered or gradated resources

We then tested whether some degree of predictability in resource distribution – as evinced by clustering or gradients of distribution – would allow the fungus to increase its fitness by using its foraging strategy. Simulations with spatially random point distribution with clustering (CSRC), with gradients (CSRG) and clustering and gradients (CRSCG) were investigated for the standard three combinations of D, F and R, giving 27 simulation types for each spatial model. In every case, the mean ΔA was positive and significantly different from zero, indicating that the ESR model acquired more resources than the UR one on average (Table 3). However, all three models generated simulations where ΔA was negative, indicating that not all spatial patterns were reacted to adaptively. The most extreme values of ΔA were −10.1 and +12.4. Figure 5B1–D3 shows the evolution of foraging fronts for three realizations of each spatial model: each example is taken from the parameter combination giving the median ΔA response and simulations representing the first, second and third quartile are shown. The figures show a very general trend to greater asymmetry with increasing foraging effectiveness.

The CSRC model performed better than the CRCG model both in terms of the overall mean response and the

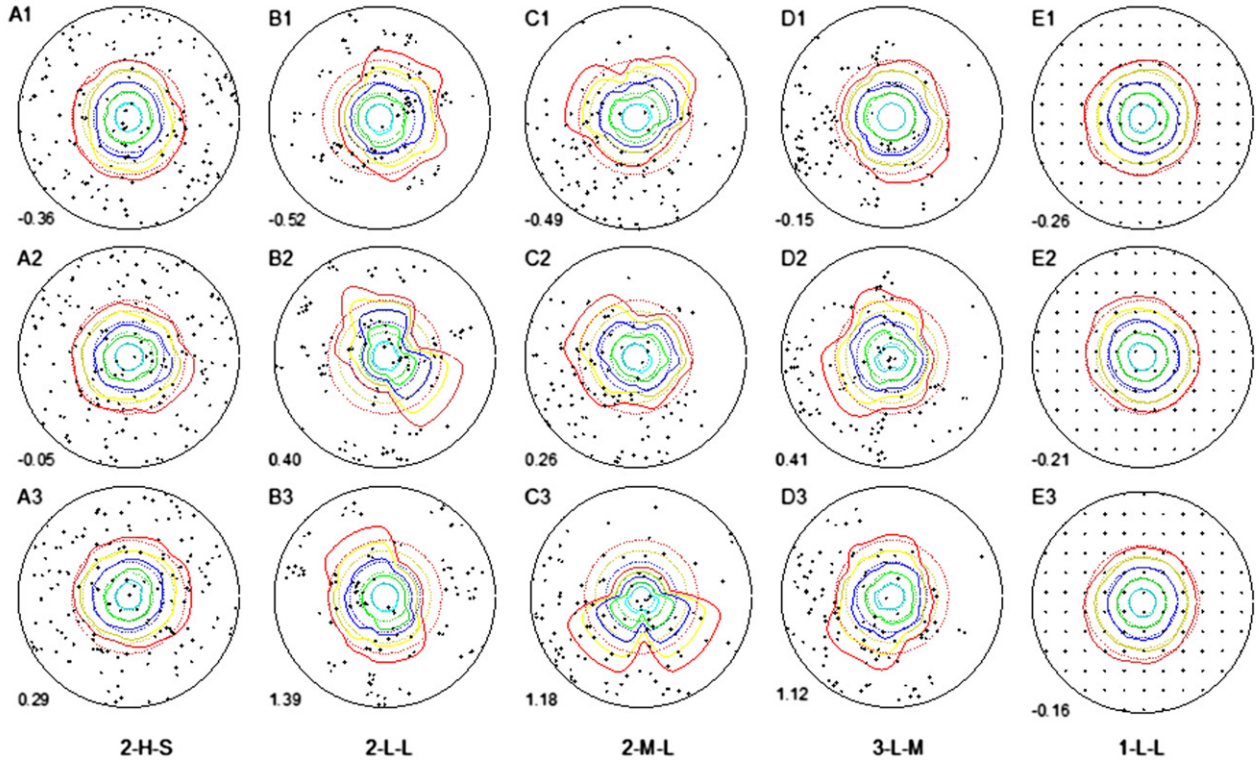

Fig. 5. Simulated development of colonies produced by the UR (dotted colour lines) and ER (same colour; solid lines) at various times after growth was initiated at the centre of the unit circle (20 = cyan; 40 = green; 60 = blue; 80 = yellow; 100 = red time steps). Black points show the location of resources that are distributed either (A) randomly, (B) as random clusters, (C) randomly but with the distribution increasing along a gradient and (D) randomly clustered and increasing along a gradient. Five hundred simulations were run for each of three different combinations of foci number (1, 2 or 3), resource density (low, medium and high) and duration of response (short, medium and long), and each vertical set of panels represents the parameter combination that gave the median, mean response out of the 27 possible combinations. The median mean for the A panels, for example, was with two foci at high density and short duration (coded as 2-H-S on the figure). A2 shows the second quartile (mean) response for the 500 2-H-S simulations while A1 and A3 were the first and third quartiles responses, with A1 favouring the uniform response model and A3 the excitable response model. First, second and third quartiles are also shown for the other distributions simulated.

Table 3. Mean performance of the ESR vs. the UR model in terms of average capture efficiency (ΔA) for different spatial distributions of resources [CSR, CSRC, CSRG and CSRCG and regular lattice (L)].

	CSR	CSRC	CSRG	CSRCG	L
Mean	0.00 ± 0.01	0.56 ± 0.03	0.38 ± 0.02	0.59 ± 0.03	−0.25 ± 0.00
Best mean	–	0.91 ± 0.18	0.74 ± 0.12	1.00 ± 0.12	–
Range	−4.6 to 4.6	−10.1 to 12.4	−3.9 to 10.0	−8.8 to 11.0	−1.0 to 0.8
IQ	−0.9 to 0.8	−1.2 to 2.0	−1.3 to 2.1	−1.9 to 2.8	−0.6 to 0.1
p(D)	0.875	0.001	< 0.001	< 0.001	< 0.001
p(F)	0.657	< 0.001	0.005	< 0.001	< 0.001
p(R)	0.411	0.008	< 0.001	< 0.001	< 0.001
p(DxF)	0.772	0.214	0.806	0.920	< 0.001
p(DxR)	0.453	0.454	0.056	< 0.001	< 0.001
p(FxR)	0.276	0.098	0.185	0.784	< 0.001
Mean SD	0.61 ± 0.12	1.57 ± 0.20	0.95 ± 0.21	1.70 ± 0.26	0.12 ± 0.02
Mean Skew	0.68 ± 0.14	0.79 ± 0.15	0.96 ± 0.14	0.77 ± 0.16	0.56 ± 0.15

Twenty-seven different parameter combinations of response duration (D), number of foci (F) and resource density (R) were investigated with 500 different, randomly generated patterns for each combination. All means are reported with 95% confidence intervals. The best mean represented the highest mean of the 27 parameter combinations. The range and lower and upper quartile (IQ) values refer to the entire dataset of 13 500 values. A three-way analysis of variance of ΔA on the entire dataset resulted in the probability values, p(X) shown for each factor and each primary interaction.

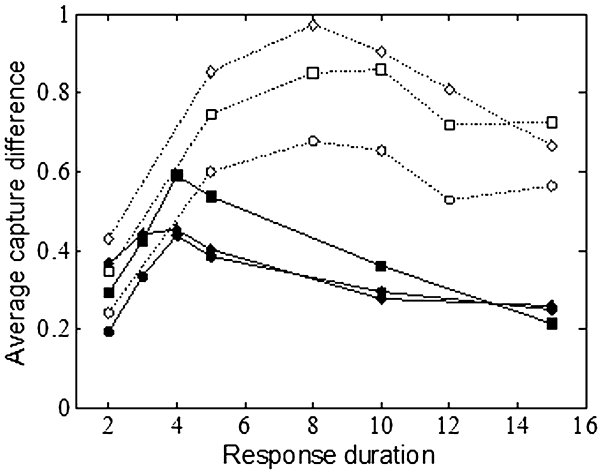

Fig. 6. Average capture difference as a function of the response duration of the bulge (time steps) for (○) low, (□) medium or (◊) high resource densities, and for 1 (filled solid line) or 3 (open dotted line) permitted simultaneous foci. Each point represents the average of 500 simulations, with different patterns of completely randomly scattered resources with clustering (see text).

highest mean response (Table 3). The CSRCG model performed best overall, although it was not significantly better than the CSRC model. In all three spatial cases, the *D*, *F* and *R* parameters were all significant predictors of the outcome (Table 3), and in the CSRCG case, there was a highly significant interaction between response duration and resource density.

The adoption of very simple foraging rules proved to be extremely efficient in acquiring resources if the resources themselves showed any spatial autocorrelation. The perimeter response was particularly efficient for clustered resources – perhaps not surprising because both are localized phenomena and operate at a similar scale. The segment response was less efficient at tracking a linear gradient in resource distribution – perhaps because the penalty to be paid for responding to a resource in the wrong direction was greater than that for a resource that was not significantly clustered. The finding that parameter values were significant predictors of outcome imply that certain parameter combinations could be subject to evolutionary selection to generate an optimal foraging strategy: this is illustrated in Fig. 6, where an extended range of response duration was simulated for two foci and the three resource densities. The results show that a *D* value of around 4 was optimal with $F = 1$ while a *D* of around 8 was optimal when up to three foci are permitted: the results also confirm the weak interactions predicted for the three parameters in Table 3.

Foraging pays high rewards but also involves high risks

Mean dispersion varied between the models (Table 3), with the gradient case having considerably less dispersion than the other two cases. In general, the better strategies had larger dispersions, indicating that the riskiness of the strategy scaled with the mean success. All three parameters were significant predictors of dispersion, although only *D* and *R* predicted skew. There were also some complex interactions between parameters for dispersion, although not for skew (Table 3).

In general, dispersion tended to increase with reward such that deploying the foraging strategy in situations where resources were clumped increased the risk of a more extreme negative pay-off – the strategy was still more favourable overall, but it was more risky for an individual colony. We were not expecting to see the dispersion reacting to different parameter combinations: for example, the nearly linear reaction to changes in response duration seen in Fig. 6. This means that both more extreme positive and negative outcomes were increasing with response duration with no corresponding effect on mean outcome. In such an environment, it is difficult to predict whether evolutionary forces would favour risky or conservative strategies, i.e. high or low *D* values.

Foraging is maladaptive for regularly spaced resources

We were also interested in the response to a very predictable resource distribution as might be used in an experimental design. For resources distributed in a regular lattice pattern, all parameter combinations gave means that were negative and significantly different from zero (Table 3): hence, the ESR strategy appears to be maladaptive when foraging for resources with a very predictable distribution. Figure 5E1–E3 shows the simulations representing the first, second and third quartiles for the median parameter combination: all three simulations are more symmetrical than any of the randomly distributed resource examples and have negative ΔA confirming that foraging was maladaptive. For this median parameter combination, only two positive ΔA were found out of the 500 patterns investigated.

The foraging rules were surprisingly maladaptive for resources distributed in a highly regular pattern. This counter-intuitive result has serious implications for experimental design because it would be natural to lay out resources in a regular grid pattern when conducting such experiments – it would seem that this is the worst possible way of assessing the foraging ability of a fungus.

Discussion

Dead wood on the forest floor serves as the resource for wood-decomposing fungi, and they are the major decomposers of it. Coarse woody debris (CWD) encompasses

everything from small twigs and wood fragments to large branches and fallen trees. Large amounts are typically present, e.g. a major review by Harmon and colleagues (1986) found that CWD averaged 39 ± 10 Mg ha^{-1} for coniferous and 18 ± 4 Mg ha^{-1} for deciduous forests with large species and site effects. The rate of decomposition of this resource, which is performed principally by fungi, is thus of considerable concern for atmospheric CO_2 concentrations.

As well as size heterogeneity, CWD is known to be spatially heterogeneous and have a clustered distribution. For example, 39% of CWD occurred in 10 out of the 80 0.04 ha plots in old growth mixed forest (Muller and Liu, 1991). High levels of spatial variation in twig and branches of oak and beech was reported by Swift and colleagues (1984), which are typical of aggregated distributions. Most data relate to downed logs because of their commercial importance, and many studies have reported strong spatial clustering.

The largest organism on earth is thought to be a species of Armillaria, covering 965 hectares with two identical genets shown to be as much as 3810 m apart. Connectivity via translocation of phosphate over distances of 1 m has been found in cord-forming saprotrophic fungi (Wells and Boddy, 1995) while interconnection of mycorrhizal systems has been shown on a similar scale (Selosse *et al.*, 2006). Observations of the physical continuity of excavated mycelial cords also support a spatial scale around the order of metres (Thompson and Rayner, 1983). Different species have been shown to operate at different spatial scales (Agerer, 2001; Genney *et al.*, 2006).

The effective ecological scale for foraging by an individual fungal colony is unknown but is likely to range from millimetre to metre. Survival of the colony must depend on the colony encountering a new resource before existing ones are exhausted, and effective foraging must be under strong selection in some conditions. The mean differences in foraging effectiveness found in the simulation studies were quite small but are still likely to be important from an evolutionary perspective. In addition, it should be noted that successful capture of a resource in the simulations did not lead to any increase in growth or surface area of the colony: this was a deliberate choice to keep the model simple and to mimic the response of the experimental system. However, it is likely that in real-world situations with greater levels of nutrient stress, the capture of a new resource would lead to an increase in the rate of growth and there would be a positive feedback between the foraging strategy and future success at resource capture. This would strengthen the conclusion that this fungus has an adaptive foraging strategy.

While the simulation modelling strongly supported *P. velutina* having an adaptive foraging strategy, directly testing this experimentally will be very challenging. Growing and simultaneously visualizing metre scale fungal colonies is not easy. The large variability of outcome means that many resource patterns yield negative foraging outcomes even though the strategy is positive overall – many colonies would have to be screened to detect the rather small differences predicted to occur between the two strategies.

Experimental procedures

Growth on scintillation screens

Fungal growth in small artificial microcosms was visualized using a non-metabolizable ^{14}C tracer Tlalka and colleagues (2008). Briefly, *P. velutina* was grown from a precolonized, central, 12 mm diameter, agar disc across an inert scintillation screen [Lite Plus or BioMax TranScreen LE (Sigma, Poole, UK)]. In some treatments, a 13 mm cellulosic bait (Grade AA filter paper disc, Whatman, Maidstone, England) or a 13 mm glass fibre disc (GF/C, Whatman, Maidstone, England) was added 20–30 mm away from the inoculum. The experiments were housed in sealed 120 mm square Petri dishes maintained at near 100% humidity at a temperature of 21 ± 0.5°C in continuous darkness.

Twenty to twenty-five microlitres (46.3 kBq) of a 0.9 mM solution of 2-amino[1-^{14}C]isobutyric acid, ^{14}C-AIB (Amersham plc, Amersham, UK) in distilled water (specific activity 2.11 GBq mmol^{-1}) was applied to the centre of the inoculum at the start of the experiment. ^{14}C-AIB was imaged using a high-resolution, photon-counting camera system (HRPCS-3, Photek, St Leonards-on-Sea, UK) equipped with a 28 mm f/2 lens as described previously (Tlalka *et al.*, 2003). The nominal (*x, y*) pixel dimensions were 588 μm and a field of view was 433×334 mm. Data were recorded continuously and integrated for 1 h per time frame.

Image processing

The outline of the colony was determined at hourly intervals by grey-level segmentation of the AIB image as described in Tlalka and colleagues (2008). The centroid of the mean of the first five images was used to determine the centre of the image. The centre was re-estimated using the same procedure at the time of bait addition. The distance to the perimeter was then estimated from the centre along 360 equally spaced angular intervals for each time frame, and this vector was used in all the subsequent analyses.

Detection of perimeter responses

Perimeter convexities were detected by identifying continuous regions of the perimeter where the radius exceeded the median radius by more than 8% using a peak detection algorithm. This radius threshold was empirically determined by inspection and represented a compromise – a low threshold detected very many, small, transient peaks while a high threshold destroyed the continuity of obvious large peaks over the time series. The angular width of the convexity was

theoretically defined by the two transitions back to the median radius: in practice, a value of 5% of the maximum length of the bulge was used for this transition to avoid the width being overly sensitive to noise. Each convexity was characterized by a maximum length and an angular width. The angular direction was determined at the midpoint of the bulge.

During the analysis of time series, bulges were classified from one time frame to the next by choosing the peak identity that maximized the amount of overlap between the two bulges. If there was no overlap, then a convexity was given a new identifier: bulges that persisted for less than 10 time steps were discarded. The dominant convexity was identified as the one with the greatest cumulative area.

Image normalization

Normalized perimeter distances (NPDs) were generated by dividing perimeter lengths by the median perimeter for each time frame. For each dataset, the mean NPD (MNPD) was calculated as the average NPD over time for each angle: note that for a symmetrically growing colony, this procedure would yield a circle of unit radius. A typical composite image represented around 150 individual image frames acquired over some 6 days: this form of analysis minimized the contribution from short-lived bulges and allowed long-term trends to be detected. The normalization was applied to the time series before and after resource addition to give two composite perimeters pre-MNPD and post-MNPD respectively. These were then smoothed with a circular median filter of length 3 to remove high frequency noise. This procedure allowed samples containing up to 185 time frames of noisy data to be condensed into a single composite dataset, both simplifying and improving the discrimination power of the analyses.

Estimation of colony areas

Colony areas were estimated for each time frame and an equivalent radius, R_e, calculated for a circular colony of the same area. Colony GRs were estimated by linear regression of R_e over time: the regression statistics indicated ($P < 0.0001$) that linear fitting was acceptable in all cases. GRs were coded by treatment and as pre- or post-bait addition.

Estimating the GR of convexities

Convexity GRs were estimated by linear regression of maximum convexity radius over time. Only post-bait data were used. A complicating feature was that some bulges did not grow immediately after bait addition and some subdominant peaks stopped growing before the end of the experiment. To account for such biphasic behaviour, two regression lines were fitted to the data by systematically altering the proportion of points contributing to each regression and selecting the analysis with the smallest residual error. Then, if the ratio of the two regression slopes was greater than 1 order of magnitude indicating that the behaviour was markedly biphasic, the greater of the slopes was taken as the bulge GR; otherwise, the single regression slope was used.

Derivation of a model of a foraging strategy for wood-decomposing fungi

Any strategy has to be compared with a default condition: the default condition here is the usual paradigm of a fungus displaying radial symmetry as it grows (Prosser and Trinci, 1979). It was then assumed that growth was not resource limited, i.e. that resource acquisition did not cause the colony to grow faster. Therefore, any enhanced GR of part of the perimeter would be matched by a decreased GR over the rest of the colony margin such that the area covered would be the same as the default radial case.

The simplest model for a fungal foraging strategy would then involve:

i. perception of a stimulus signalling the availability of a resource. Wood is insoluble so we assume that it is perceived by contact that then triggers a perimeter response;
ii. translation of the segment response into an enhanced GR over part of the perimeter;
iii. maintenance of the enhanced growth for long enough to distort the shape of the colony and break radial symmetry.

This segment growth response was captured mathematically using a three-parameter model termed the ESR model. The parameters are:

i. the enhanced GR relative to rest of the colony (G);
ii. the angular length of the responding segment (W);
iii. the centrally aligned proportion (P) of W, which grows at G (if $P < 1$, the remainder of the perimeter was fitted by a sine function connecting the excited segment to the remainder of the unresponsive colony margin).

Two further parameters were required to fully describe the foraging behaviour of the colony: the duration of the ESR (D) and the number of such segment foci (F) that a colony could simultaneously support. If the segment contacted a new resource within this period, the duration was restarted: it was therefore possible for an excited segment to remain in existence for the duration of the entire simulation. Where F was constrained, it was assumed that the excited segment(s) inhibited other parts of the perimeter from reacting to new resources while it (they) remained in existence. Simulations were conducted to assess the sensitivity of the model to D and F. For presentation, all perimeter data were normalized to the unit circle. The simulation models had an arbitrary spatial scale as the actual scale simply depended on the length and number of time steps.

Scoring relative foraging efficiency

To investigate whether the ESR foraging model was adaptive, a number of resources were randomly scattered on the plane, and each model was allowed to explore the resulting spatial pattern for 100 time steps. The relative success of the models was scored using two statistics.

$$\Delta A = \frac{\sum_{i=j}^{100} (E_i - U_i)}{(100 - j)} \quad (1)$$

Average capture difference, ΔA, represented the average difference in the number of resources acquired by the

models, where *Ei* and *Ui* were the cumulative number of resources acquired by the ESR and UR models respectively at the *i*th time point. *j* denotes the time point when the first resource was encountered.

$$\Delta C = E_{100} - U_{100} \quad (2)$$

The cumulative capture difference, ΔC, was the difference in the number of resources captured by the two models at the end of the simulation.

Different stochastically generated patterns of resource distribution were investigated (Snyder and Miller, 1991). A spatial Poisson process was used to generate CSR patterns of fixed resource density on the unit circle. CSRC used a spatial Poisson process with Neyman–Scott clustering. CSRG were generated by a non-homogeneous Poisson process. All these methods used pruning to achieve constant resource densities on the unit circle. Where resources were distributed on a regular lattice, a stochastic variable determined where in the central grid square the origin was placed, and the whole grid was then shifted to centre the unit circle on this origin. This procedure inevitably meant that resource densities within the unit circle varied slightly – however, this effect was only seen right at the edge of the circle and few colonies ever explored that far.

The capture of resources were simulated for three *D* (5, 10 and 15) and three *F* (1, 2 and 3) values for low, medium and high resource densities, giving 27 parameter combinations in all. Five hundred resource patterns were investigated for each parameter combination. In each case, the resources acquired by a UR model were compared with an ESR model by calculating the ΔA values for each simulation.

Model pseudo code

The basic design of the mathematical model used to simulate the UR and ESR models is shown here in pseudo code. The main experimental values that are tracked are (i) the distance of the perimeter from the centre of the colony at 1 degree intervals (stored in r) and (ii) the number of resources captured at each time step [stored in n – UR(t) and n – EST(t)].

```
  Colony perimeter radius = r(1..360); r = 0,
t = 0% create arrays with 360 elements to hold
radius values
  loop 1-5000 % simulation repeat loop
  Scatter resources randomly according to dis-
tribution model being tested via subroutine
SCATTER
  loop 1-100 % time loop
```

Uniform resource model.

```
  loop 1-360 % radius
increment loop
  r(1,360) = r((1,360) * GS % growth at stand-
ard uniform rate
  if (any r(i) contacts resource) then
  n - UR(t) = n - UR(t)+1     %     increment
resource counter for time step
  end if
  end radius loop
```

ESR model.

```
  Calculate GR via subroutine
  Loop 1 to 360 % radius increment loop
  Expand perimeter section of model
  if(excited and < D ) then % if contact
previously made less than D time steps ago
  if(centre) then % in central portion of
bulge
  r(i) = r(i) + G % grow at an enhanced rate
  else % in side portion of bulge
  r(i) = r(i) + G × f(position) % grow at a
reduced enhanced rate as a function of
      position in bulge given by sine func-
tion (range 0..1)
  end if
  else
  r(i) = r(i) + GR % not excited or no longer
excited so grow at the reduced GR calculated
by
  the subroutine GR
  end if
  if(any r(i) contacts resource) then
  n - ESR(t) = n - ESR(t) + 1   %   increment
resource counter for time step
  end if
  end radius loop
  Change excitation status of perimeter
  loop 1 to number of bulges
  if(any r contacts resource) then % if any
part of the bulge contacts a new resource
  bulge(j).duration = D % reset bulge dura-
tion to maximum for simulation
  elseif(bulge(j).duration > D) % bulge has
existed for maximum duration
  bulge(i).excited = false   %   destroy   the
bulge by marking all its rs as non-excited
  else
  do nothing % allow the bulge to continue
  end if
  end bulge loop
  loop over all r not in bulges
  if(r = resource position) % contact made
with new resource
  if(# of foci < F) then % if there are fewer
bulges than the maximum allowed
  create new bulge % centre bulge on resource
position with 0.5xW on each side
  bulge(j).excited = true % mark all the r
belonging to bulge as excited
  bulge.duration = D % mark all the r belong-
ing to bulge with duration to D
  else
  do nothing % too many foci to allow a new
bulge to form
  end if
  end all r loop
  end time loop
  score relative model success as ΔA and ΔC
  end simulation loop
```

SCATTER subroutine uses simulated random numbers to place a number of single resources on a plane. Different algorithms are used for different models of resource

distribution (see text for details). Each simulated distribution is used for the UR and ESR model.

GR subroutine iteratively calculates reduced GR by estimating the GR of all the perimeter points not currently in bulges that would be required to ensure that the area of the UR and ESR model will be the same at the current time step after all the perimeter points have expanded by GS (for the uniform model), by G or G * f(position) (for points in bulges) or GR (for points not in bulges for the ESR model).

Acknowledgements

We gratefully acknowledge financial support from the NERC (GR3/12946), BBSRC (43/P19284) and from the Dunstan Bequest (University of Oxford).

References

Agerer, R. (2001) Exploration types of ectomycorrhizae – a proposal to classify ectomycorrhizal mycelial systems according to their patterns of differentiation and putative ecological importance. *Mycorrhiza* **11:** 107–114.

Boddy, L. (1999) Saprotrophic cord-forming fungi: meeting the challenge of heterogeneous environments. *Mycologia* **91:** 13–32.

Boddy, L., Hynes, J., Bebber, D.P., and Fricker, M.D. (2009) Saprotrophic cord systems: dispersal mechanisms in space and time. *Mycoscience* **50:** 9–19.

Dowson, C.G., Rayner, A.D.M., and Boddy, L. (1986) Outgrowth patterns of mycelial cord-forming basidiomycetes from and between woody resource units in soil. *J Gen Microbiol* **132:** 203–211.

Dowson, C.G., Rayner, A.D.M., and Boddy, L. (1988) Foraging patterns of phallus-impudicus, phanerochaete-laevis and steccherinum-fimbriatum between discontinuous resource units in soil. *FEMS Microbiol Ecol* **53:** 291–298.

Fricker, M.D., Bebber, D., and Boddy, L. (2008) Mycelial networks: structure and dynamics. In *Ecology of Saprotrophic Basidiomycetes*. Boddy, L., Frankland, J.C., and VanWest, P. (eds). San Diego, CA, USA: Elsevier Academic Press, pp. 3–18.

Fricker, M.D., Boddy, L., Nakagaki, T., and Bebber, D.P. (2009) Adaptive biological networks. In *Adaptive Networks: Theory, Models and Applications*. Gross, T., and Sayama, H. (eds). New York, USA: Springer, pp. 51–70.

Genney, D.R., Anderson, I.C., and Alexander, I.J. (2006) Fine-scale distribution of pine ectomycorrhizas and their extramatrical mycelium. *New Phytol* **170:** 381–390.

Harmon, M.E., Franklin, J.F., Swanson, F.J., Sollins, P., Gregory, S.V., Lattin, J.D., *et al*. (1986) Ecology of coarse woody debris in temperate ecosystems. *Adv Ecol Res* **15:** 133–302.

Hutchings, M.J., John, E.A., and Stewart, A.J.A. (eds) (2000) *The Ecological Consequences of Environmental Heterogeneity*. Cambridge, UK: Cambridge University Press.

James, A., Plank, M.J., and Edwards, A.M. (2011) Assessing Lévy walks as models of animal foraging. *J R Soc Interface* **8:** 1233–1247.

de Kroon, H., Huber, H., Stuefer, J.F., and van Groenendael, J.M. (2005) A modular concept of phenotypic plasticity in plants. *New Phytol* **166:** 73–82.

Lynch, J.P., and Brown, K.M. (2012) New roots for agriculture: exploiting the root phenome. *Philos Trans R Soc Lond B Biol Sci* **367:** 1598–1604.

MacArthur, R.H., and Pianka, E.R. (1966) On optimal use of a patchy environment. *Am Nat* **100:** 603–609.

Mardia, K.V., and Jupp, P.E. (2000) *Directional Statistics*. Chichester; New York: J. Wiley.

Muller, R.N., and Liu, Y. (1991) Coarse woody debris in an old-growth deciduous forest on the Cumberland Plateau, southeastern Kentucky. *Can J For Res* **21:** 1567–1572.

Prosser, J.I., and Trinci, A.P.J. (1979) Model for hyphal growth and branching. *J Gen Microbiol* **111:** 153–164.

Pyke, G.H. (1984) Optimal foraging theory: a critical review. *Annu Rev Ecol Syst* **15:** 523–575.

Rayner, A.D.M., and Franks, N.R. (1987) Evolutionary and ecological parallels between ants and fungi. *Trends Ecol Evol* **2:** 127–133.

Ripley, B.D. (1976) 2nd-order analysis of stationary point processes. *J Appl Probab* **13:** 255–266.

Selosse, M.A., Richard, F., He, X.H., and Simard, S.W. (2006) Mycorrhizal networks: des liaisons dangereuses? *Trends Ecol Evol* **21:** 621–628.

Snyder, D.L., and Miller, M.I. (1991) *Random Point Processes in Time and Space*. New York, USA: Springer-Verlag.

Swift, M.J., Boddy, L., and Healey, I.N. (1984) Wood decomposition in an abandoned beech and oak coppiced woodland in SE England. 2. The standing crop of wood on the forest floor with particular reference to its invasion by tipula flavolineata and other animals. *Holarct Ecol* **7:** 218–228.

Thompson, W., and Rayner, A.D.M. (1983) Extent, development and function of mycelial cord systems in soil. *Trans Br Mycol Soc* **81:** 333–345.

Tlalka, M., Hensman, D., Darrah, P.R., Watkinson, S.C., and Fricker, M.D. (2003) Noncircadian oscillations in amino acid transport have complementary profiles in assimilatory and foraging hyphae of *Phanerochaete velutina*. *New Phytol* **158:** 325–335.

Tlalka, M., Bebber, D.P., Darrah, P.R., Watkinson, S.C., and Fricker, M.D. (2008) Quantifying dynamic resource allocation illuminates foraging strategy in *Phanerochaete velutina*. *Fungal Genet Biol* **45:** 1111–1121.

Trinci, A.P.J. (1971) Influence of width of peripheral growth zone on radial growth rate of fungal colonies on solid media. *J Gen Microbiol* **67:** 325–344.

Watkinson, S.C., Bebber, D., Darrah, P.R., Fricker, M.D., Tlalka, M., and Boddy, L. (2006) The role of wood decay fungi in the carbon and nitrogen dynamics of the forest floor. In *Fungi in Biogeochemical Cycles*. Gadd, G.M. (ed.). Cambridge, UK: Cambridge University Press, pp. 151–181.

Wells, J.M., and Boddy, L. (1995) Phosphorus translocation by saprotrophic basidiomycete mycelial cord systems on the floor of a mixed deciduous woodland. *Mycol Res* **99:** 977–980.